DOI: https://doi.org/10.14256/JCE.3539.2022
Građevinar 2/2023

Primljen / Received: 30.5.2022.
Ispravljen / Corrected: 19.8.2022.
Prihvaćen / Accepted: 6.11.2022.
Dostupno online / Available online: 10.3.2023.

Alternate approach for calculating the optimum viscous damper size

Author:

Assoc.Prof. **Elif Cagda Kandemir**, PhD. CE
Izmir Demokrasi University, Turkey
Faculty of Civil Engineering
elifcagda.kandemir@idu.edu.tr
Corresponding author

Research Paper

Elif Cagda Kandemir

Alternate approach for calculating the optimum viscous damper size

This study explores the optimal viscous damper size required to prevent a five-story building from colliding with a rigid wall. It comprises two parts, both based on the novel application of the wavelet coherence method (WCoh). In the first, impact incidents were estimated using the WCoh method, and in the second, an approach based on WCoh for optimizing the viscous damper size was proposed. A validation model was used to verify the proposed method and good agreement among total damper sizes was observed. Nonlinear viscous dampers have also investigated due to their lower damping force than viscous dampers produce. This study has shown that wavelet coherence can be used to identify seismic pounding.

Key words:
seismic pounding, viscous damper, continuous wavelet transform (CWT), wavelet coherence (WCoh), near-fault ground motions

Prethodno priopćenje

Elif Cagda Kandemir

Alternativni pristup za izračunavanje optimalne veličine viskoznog prigušivača

Ovaj rad istražuje optimalnu veličinu viskoznog prigušivača potrebnu za sprječavanje sudara peterokatnice s krutim zidom. Sastoji se od dva dijela, oba temeljena na novoj primjeni metode wavelet koherencije (WCoh). U prvom su dijelu slučajevi udara procijenjeni metodom WCoh, a u drugom je predložen pristup temeljen na metodi WCoh za optimizaciju veličine viskoznog prigušivača. Za provjeru predložene metode korišten je validacijski model i primijećeno je da se ukupne veličine prigušivača dobro slažu. Nelinearni viskozni prigušivači imaju omjer prigušenja koji je identičan onom linearnih viskoznih prigušivača, ali imaju nižu silu prigušivanja, čime štite konstrukciju i prigušivač pri velikim brzinama konstrukcija. Ovo je istraživanje pokazalo da se wavelet koherencija može koristiti za identifikaciju seizmičkog sudara.

Ključne riječi:
seizmički sudar, viskozni prigušivač, kontinuirana wavelet transformacija (CWT), wavelet koherencija (WCoh), gibanja tla u blizini rasjeda

1. Introduction

Migration from villages to cities for better living conditions not only increases population in cities but also reduces the amount of land that can be used for residential development. Hence, metropolitan areas often have adjacent buildings with little space separating them. In Figure 1, adjacent buildings with no seismic gap can be seen on one of the main arteries in Izmir, which is the third largest city in Turkey. The city lies in an active seismic zone; hence, it has experienced severe earthquakes in the past, and in 2020, it was exposed to the Aegean Sea earthquake.

Adjacent buildings are susceptible to serious damage during earthquakes because of the aforementioned insufficient gaps and unsynchronized behaviour of neighbouring structures. For decades, researchers have investigated issues related to seismic events in all aspects: optimal gaps between neighbouring structures [1–5], analytical models for seismic forces [6–13], methods for mitigating the effects of earthquakes [14–19], and so on. Although there is a considerable interest in the subject [20–24], there are issues for which researchers have not reached a consensus and their solutions remain undetermined.

Recently, signal processing methods have attracted attention from researchers who are familiar with structural engineering subjects. Wavelet transform, which provides the frequency content of a time signal, has better window function scaling and shifting than Fourier transforms [25]. Mohebi et al. [26] used complex Morlet mother wavelet to perform continuous wavelet transform (CWT) and detect damage due to seismic forces. Xing et al. [27] performed a wavelet transform on the acceleration responses of a single-degree-of-freedom (SDOF) structure colliding with a rigid barrier to detect pounding and verified the method experimentally. Young Noh et al. [28] conducted the CWT of seismic responses considering only the first mode to detect structural damage, and Yazdanpanah et al. [29] improved the method using complex Morlet and higher mode contributions to determine fragility curves and estimate structural health.

The method proposed in this study is easy to understand and can be used in the preliminary design of viscous dampers. It aims to regulate the seismic responses of structures with the aid of viscous dampers by simulating their responses with optimal gaps based on the frequency of their responses. Numerous studies focus on the size and/or location of viscous dampers in buildings. De Domenico et al. [30] reviewed interstorey viscous damper installation methods. The purpose of their study is to decrease or limit seismic responses by increasing the overall damping ratio using stochastic and optimization methods with different approaches and constraints. In addition, Silvestri et al. [31] proposed a different installation scheme, called "fixed point", for viscous damper sizing by connecting all dampers to the ground, different from this study in this aspect, defined in a five-step procedure. The proposed approach uses only the seismic responses obtained by numerical methods to determine the interstorey viscous damper size after processing them using wavelet-based methods.

Impact models require numerical analysis to obtain the impact force and its time based on numerous coefficients of colliding surfaces and their geometry; however, the proposed method can be used to find impact incidents by comparing the seismic responses obtained for structures with and without adequate seismic gaps based on the wavelet coherence technique.

This study presents a promising method for determining the optimal damper size required to prevent pounding. First, the wavelet coherence approach for evaluating pounding behaviour based on the CWT was exhibited. This procedure was followed by optimization viscous dampers to prevent pounding. For the optimisation, the objective function is assigned as minimized total damper coefficient. Considering that the structure becomes elastic after dampers are added, the linear elastic behaviour of the building was considered [31, 32]. Two models were employed in this study: one proposed by Lavan and Levy [32] for validating the proposed method and another by Kandemir-Mazanoglu and Mazanoglu [33] for parametric analysis under various gap distances and earthquake motions. Linear and nonlinear viscous damper sizes were implemented for a five-storey building, and the results were compared.

2. Problem formulation

This section presents the objectives, methodology, and optimization approach of the proposed method. The aim of this study is to determine the viscous damper size for a five-storey building that prevents one-sided impact on a rigid wall. The dampers were implemented horizontally between consecutive floors considering a uniform damper size distribution. This study uses the frequency changes of system responses to evaluate pounding and viscous damper sizes. Within the scope of this study, wavelet transform, which is a powerful technique for detecting the frequency information of a signal, was used after the wavelet coherence method.

Figure 1. Adjacent buildings in Izmir

2.1. WCoh method and structural pounding relation

Impact forces acting on a structure are activated when a seismic gap is closed at an unpredicted moment. Owing to the randomness of impact forces, structural responses are nonlinear in a structure's elastic range. The equation of motion for a multi degree-of-freedom model subjected to one-sided pounding is $[M]\{\ddot{X}\} + [C]\{\dot{X}\} + [K]\{X\} + \{F_p\} = -[M]\{1\}\, \ddot{x}_g$, where [M] is the mass matrix, [C]is the damping coefficient matrix, and [K]is the stiffness matrix while $\{\ddot{X}\}$, $\{\dot{X}\}$ and {X} are the acceleration, velocity, and displacement responses of the structure, respectively. $\{F_p\}$ includes the pounding forces of each floor that has active and passive states associated with closed and open gaps, respectively. A passive state occurs when there is no pounding. If there is pounding, that is, an active state, the value of the force depends on the selected model. In related literature, there are many models that can be used to simulate gap elements that produce impact forces [34-37]. Gap-activated stiffness and/or damping are added to the structure, and the natural frequency changes during impact. At this point, wavelet transform can be used after the wavelet coherence method and to observe frequency differences between structures with and without an adequate seismic gap.

Recently, signal processing techniques, including wavelet-based approaches, have become significant in structural engineering [38-40]. Before discussing the WCoh method, we first briefly introduce the wavelet transform. Wavelet transforms are more suitable for providing simultaneous frequency-time information for non-stationary signals than Fourier transforms owing to its adaptive windowing technique. It decomposes the signal into basic functions of dilated (scaled) and translated (shifted) versions of the mother wavelet function. There are two types of wavelet transforms: discrete and continuous. The discrete wavelet transform (DWT) uses only a subset of scale and shifting parameters while CWT computes wavelet coefficients at each scale in discrete time. Despite its heavy computational load, the latter has been used in this study owing to its adaptive windowing capability to provide frequency information. Wavelet coefficients, $C(a,b)$, as functions of a and b, are computed by multiplying the original signal with appropriately scaled and shifted wavelets as follows [41]:

$$C(a,b) = \int_{-\infty}^{\infty} f(t)\cdot\psi(a,b,t)\,dt \tag{1}$$

$$\psi(a,b,t) = \frac{1}{\sqrt{a}}\psi^{*}\cdot\left(\frac{t-b}{a}\right) \tag{2}$$

Where $\Psi(a, b, t)$ is the main wavelet and t, a, and b are time, scale, and shifting factors, respectively. Ψ^* is a complex conjugate of the wavelet. The scale parameter (a) is inversely proportional to the frequency. Consequently, the correlation coefficient of the scaled wavelet with the signal is plotted on the frequency–time plane. The scalogram of CWT shows the correlation between the scaled (a) and shifted (b) wavelet and signal. Abrupt variations in the signal can be detected with high frequency, while slower ones can be detected with low frequency. Wavelets have different forms, such as Haar, Morlet, Daubechies, and Mexican Hat. The Morlet wavelet, which was used in this study, is a complex function that has been shown to be effective for frequency extraction for signals diagnosis, [42, 43]. It has also been applied in seismic signal detection [44, 45]. Wavelet coherence is a method that represents the frequency synchronisation of two time series in a certain time range. The coherency coefficients (WCoh) are calculated using the following equations:

$$WCoh = \frac{\left|S\left(C_x^{*}(a,b)C_y(a,b)\right)\right|^2}{S\left(\left|C_x(a,b)\right|^2\right)\cdot S\left(\left|C_y(a,b)\right|^2\right)} \tag{3}$$

$$\Delta\varphi(t,a) = \tan^{-1}\frac{\mathrm{Im}\left[W^{XY}(t,a)\right]}{\mathrm{Re}\left[W^{XY}(t,a)\right]} \tag{4}$$

where $C_x(a,b)$ and $C_y(a,b)$ represent the CWTs of the x and y signals at a scales and b positions. The superscript * is the complex conjugate and S is the operator for smoothing the time and scale parameters. In the formulation, the cross-wavelet term ($C_x^*(a,b)C_y(a,b)$) is included in the numerator. $\Delta\Psi$ denotes the phase of the wavelet. The coefficients are plotted in the frequency–time space while the phase is indicated by arrows. Wavelet coherence takes values between zero and one to represent dissimilarity and similarity, respectively. For WCoh, zero and one represent completely different and exactly matching frequency content, respectively. For detailed information about the subject, please refer to Torrence and Compo [25] and Grinsted et al. [46].

In this study, the wavelet coherence method has been applied to acceleration responses due to earthquake ground motion when the structure has adequate and inadequate seismic gaps. A Wcoh value different from one indicates different frequency contents of responses; thus, pounding occurs. After installing viscous dampers between the consecutive floors in the building structure, as no pounding is expected, the frequency contents of the seismic responses become equivalent to those when the system has an adequate seismic gap, that is no pounding state, resulting one for Wcoh value. The equation of motion was solved using Newmark's step-by-step method with a constant average acceleration and time step of 0.001 s. This was done to obtain the acceleration responses of structures with and without pounding.

2.2. WCoh-based optimization of viscous damper size

This section describes the procedure for determining the optimum viscous damper size that prevents pounding. The wavelet coherence method explained in the previous section stores the coefficients in a matrix with the size of period × duration. For a complete signal coherency, all coherence coefficients must be equal to one at each period. Therefore, a new parameter, called the average wavelet coherence coefficient (AWC), was introduced. AWC is calculated according to Eq. (5), where *T* is the duration of the signal, *i* is the period, and *WCoh coefficient* is the corresponding period.

$$AWC_i = \frac{\sum_{t=0}^{T} \left(WCoh\,coefficient\right)_t}{T} \tag{5}$$

The procedure followed in this paper is given by the flowchart in Figure 2. The objective function is the minimum total damper coefficient ($Cd = \Sigma c_d$). An inequality constraint applies lower (*lb*) and upper (*ub*) bounds to the damper coefficient (c_d) of each damper installed at each floor ($lb \leq c_d \leq ub$). *lb* is zero for the case without and damper and *ub* is 3 × 10⁶ Ns/m. The equality constraint is that the average wavelet coherence must be one (AWC = 1). The optimization process can be summarized as follows:

Step 1. Input the structural data as mass, stiffness, and damping matrices. The damping matrix is generated by the Rayleigh damping method with a damping ratio of 5 % for the first and last modes.

Step 2. Input the additional damping ratio of viscous dampers (at first, zero is assigned for no damper state).

Step 3. Time response analysis is performed, and the acceleration responses of each floor are obtained.

Step 4. The WCoh method is applied to the CWT of the acceleration responses of the structure with and without pounding. Then, the AWC of each floor is calculated.

Step 5. If all AWCs are equal to one, time response analysis is performed to determine pounding forces using the Kelvin–Voigt model (or any other model given in literature). If there is no pounding at any floor, the algorithm is terminated, and no viscous damper is required.

Step 6. If one of the AWCs in Step 5 is not equal to one, the additional damping ratio (x_d) is gradually increased (in steps of 0.01 in this study) and the viscous damper coefficients (*cd*) of each floor between the inequality constraints are computed and introduced into the corresponding location of the structural damping matrix (*C*). Dampers are placed from the first floor onwards.

Step 7. Steps 3 and 4 and are repeated by gradually increasing x_d until the equality constraint AWC is equal to one and no pounding occurs at all floors.

Additional damping ratio (x_d) formulation for interstorey linear viscous dampers is given in FEMA 273 [52] as follows:

$$\xi_d = \frac{T_1 \sum_j cd\left(\alpha\right)_j cos^2\left(\theta_j\right)\left(\phi_j - \phi_{j-1}\right)^2}{4\pi \sum_i m_i \phi_i^{\,2}} \tag{6}$$

where T_1 is the fundamental natural period, *cd*(*a*) is the damping coefficient with a denoting the velocity exponent, q_i is zero if the damper is horizontal, and m_i indicates the mass of one floor. (ϕ_j-ϕ_{j-1}) indicates the relative horizontal modal displacements between consecutive floors at the first mode. Subscript i is used for indexing the floor while j is the floor where dampers are added. This optimization algorithm was run for two cases for the gap distances of 10 and 15 cm between the structure and rigid wall under different near-fault earthquakes.

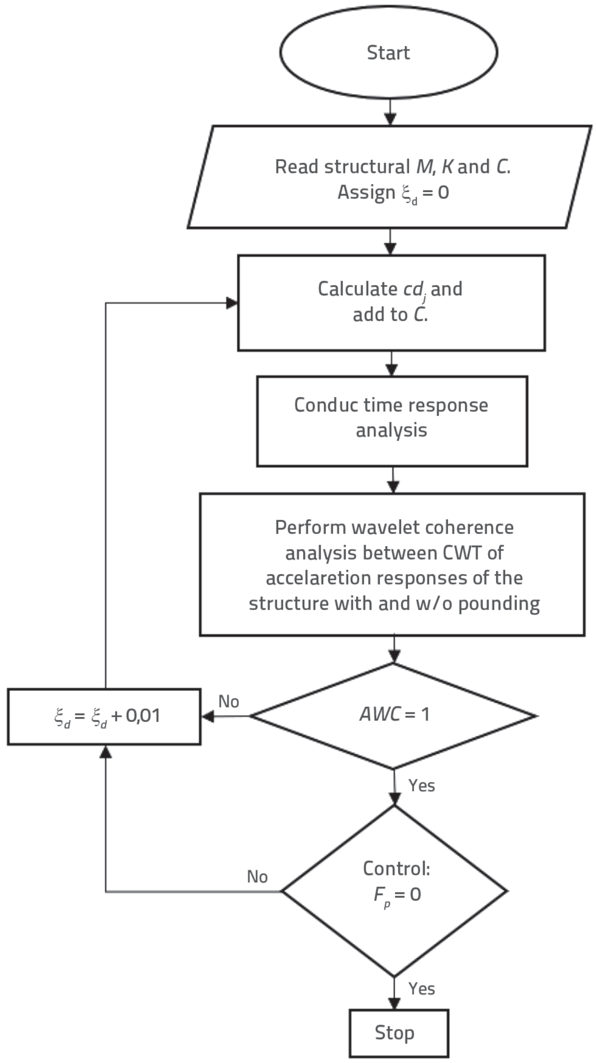

Figure 2. Flow chart of the optimization procedure

3. Ground motions

Selected ground motions are the examples of near-fault earthquake ground motions. The earthquakes were scaled according to the acceleration design spectrum of the Kocaeli province (latitude 40.696536°, longitude 29.811293°) in Turkey, for which the spectral accelerations are 2.059 and 0.694 at 0.2 and 1 s periods and the soil class is ZC (very dense soil and soft rock) [47]. Table 1 shows the properties of the selected earthquakes.

Table 1. Selected earthquake motions

Earthquake name, year	Station	Component	PGA [g]	Scale factor
Chi-Chi, 1999	TCU065	E	0.790	0.667
	TCU065	N	0.575	
Imperial Valley, 1979	Array #5	140	0.529	0.781
	Array #7	140	0.341	
Kobe, 1995	Takatori	0	0.618	0.905
	Takatori	90	0.671	
Kocaeli, 1999	Duzce	180	0.312	1.226
	Duzce	270	0.364	
Landers, 1992	Lucerne	260	0.725	1.034
	Lucerne	345	0.789	
Northridge, 1994	Rinaldi	228	0.874	0.689
	Rinaldi	318	0.472	

4. Structural model

The structure discussed in this study is a five-storey shear frame and has been idealized as the lumped mass-stiffness model. The mass and stiffness of each floor were 1×10^5 kg and 6.8×10^7 N/m, respectively [33]. The natural period of the first mode was 0.85 s. Inherent damping of 5 % was used for the first and last modes to construct a Rayleigh damping matrix. The structure was evaluated for gap distances (*d*) of 10 and 15 cm. Figure 3 shows the model.

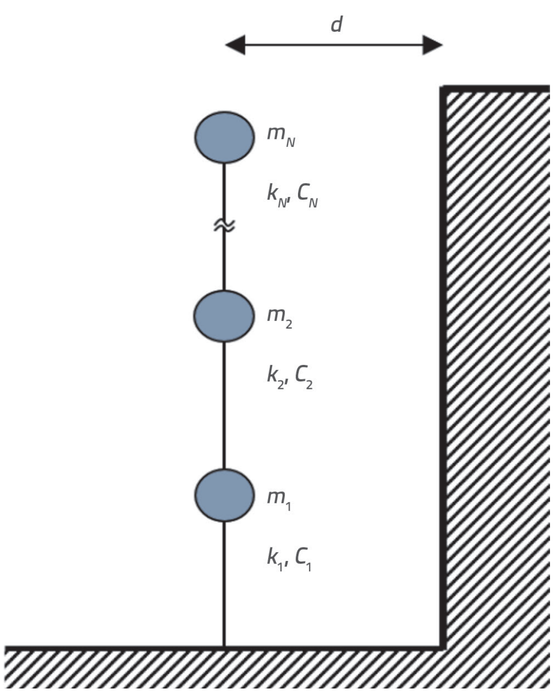

Figure 3. Lumped mass-stiffness model of the structure and rigid wall

5. Results

The results of this study are presented under two headings. The first presents the seismic pounding detected by the WCoh method, and the second presents the optimization results. Model setup and time response analysis under earthquake motion and wavelet analysis were performed in MATLAB [48].

5.1. Estimation of seismic pounding using Wcoh method

In this section, the acceleration responses for the structure with and without sufficient seismic gap were compared using the wavelet coherence method; this comparison was performed to detect frequency differences. The results of the Chi-Chi and Northridge earthquakes were examined because they had the largest impact values. The computed WCoh coefficients of roof accelerations with and without pounding were plotted against time. In the default spectrum, yellow is for high coherence and blue for low coherence. The white-dashed line shows the cone of influence without edge effects. Arrows in wavelet coherence graphs have various meanings: arrows pointing to the right indicate signals that are in phase, arrows to the left indicate a phase difference of 180°, and arrows pointing up and down indicate a phase difference of 90°. The direction of the arrows does not affect the coherence coefficients.

To verify coherence plots, pounding forces modelled using the Kelvin–Voigt model (linear spring-damper) were computed using the following equation [7]:

$$F_p(t) = k_p \delta(t) + c_p \dot{\delta}(t) \tag{7}$$

$$c_p = 2\xi_p \sqrt{k_p \frac{m_1 m_2}{m_1 + m_2}} \tag{8}$$

$$\xi_p = \frac{-\ln e}{\sqrt{\pi^2 + (\ln e)^2}} \tag{9}$$

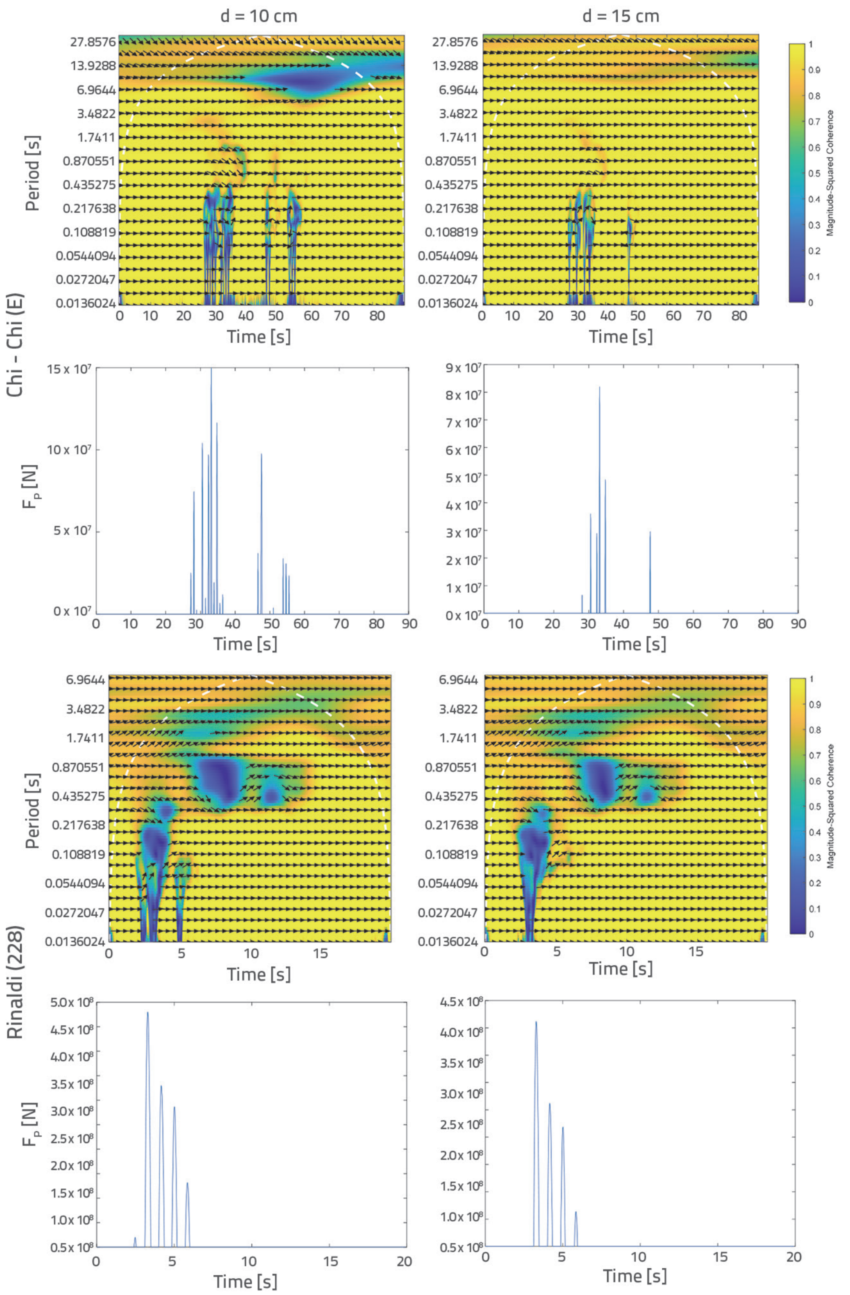

Figure 4. Wavelet coherence plots between acceleration responses with and without pounding and corresponding pounding force-time diagrams

where $F_p(t)$ is the pounding force as a function of time (t), k_p is the stiffness, and c_p is the damping coefficient of the impact model. $\delta(t)$ and $\dot{\delta}(t)$ are the relative displacement and velocity between two colliding structural members, respectively. ξ_p is the impact damping ratio and e is the coefficient of restitution. Masses of colliding members are denoted as m_1 and m_2, which are the masses of the floor of the structure (1 × 10^5 kg) and rigid wall (1 × 10^5 kg) corresponding to the adjacent building floor, respectively. In the present study, k_p was assumed to be 20 times the storey stiffness coefficient, as suggested by Anagnostopoulos [7]. Moreover, ξ_p of 0.14 (e = 0.65) was used for concrete surfaces, as suggested by Azevedo and Bento [49]. The linear spring and dashpot are activated when the gap between structures is closed, thereby generating pounding force.

Figure 4 shows the wavelet coherence and their corresponding pounding force-time graphs. The formations in the form of blue lines, which appear between 0 and 0.5 s in both earthquakes, show the collision moments. A more intense shade of blue represents a greater pounding force. The corresponding pounding force-time graphs verify the results obtained from WCoh plots. The graphs show blue areal formations in addition to the previously mentioned linear vertical formations. For example, between 0.4 and 1.5 s, areal non-coherence coefficients are observed for both gap distances during the Rinaldi earthquake. These incoherences can be said to be due to the phase difference between the behaviours after impact. Note that the arrows pointing to the right in different angles to the horizontal (up and down) indicate positively correlated signals.

5.2. Optimized total damper size

This section presents the processing of the wavelet coherence coefficients obtained in the previous section. After the WCoh analysis of acceleration responses in MATLAB, the coefficients are stored as a matrix of size period × duration. Consequently, the average values of WCoh coefficients at each period of the structure [50] were calculated as given in Eq. (5) and defined as an equality constraint in the optimization process. Figure 5 depicts the AWC-period relation for each earthquake motion in 0 to 5 s.

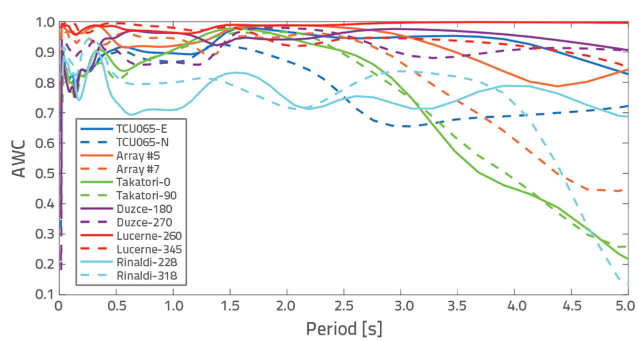

Figure 5. AWC for each period and earthquake

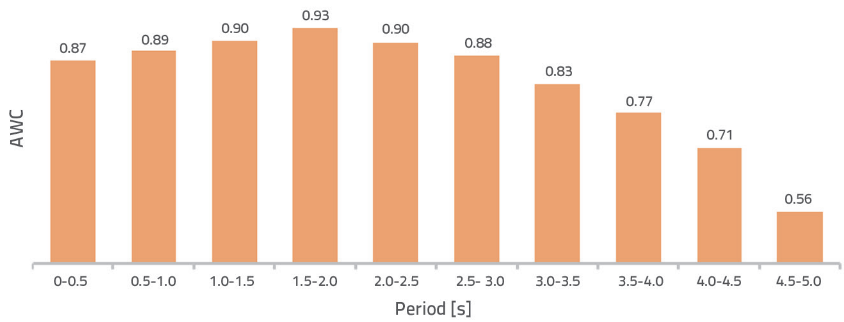

Figure 6. Average AWC with the corresponding period ranges

Figure 6 shows the average AWC with time considering all the earthquakes. The largest coherency occurs in the range 1.5 to 2 s whereas the lowest occurs in the range 4.5 to 5 s for the investigated ground motions and structure. The decrease in the average AWC with the period implies that the behaviour in higher periods is totally different when the structure has an inadequate seismic gap.

5.2.1. Validation model

The model in the study by Lavan and Levy [32] presented in Figure 7 was used to verify the proposed method. The model is a two degree-of-freedom system in which each floor mass is 25 ton. The stiffnesses of the first and second floors are 37500 and 25000 kN/m, respectively, while inherent damping coefficients are 48.609 and 32.411 kNs/m, respectively. The ground motion used is the NS component of the 1940 El-Centro earthquake scaled by 2.01.

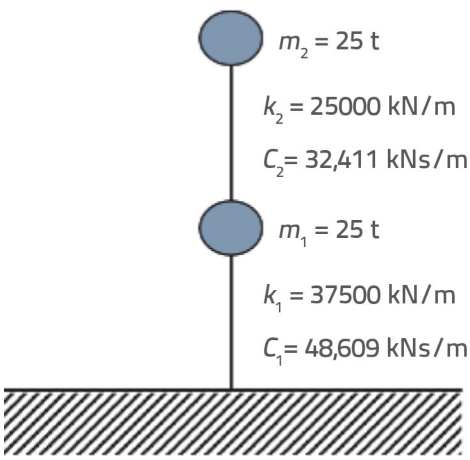

Figure 7. Validation model [32]

In the referred study, the maximum drift in the drift coordinate system was selected as 9 mm for the inequality constraint. If the drifts are transformed into displacements, the maximum allowable displacements become 9 and 18 mm for the first and second floors, respectively. Table 2 shows the comparative results of the total damper sizes. The total damper size calculated by the proposed method was 8.1 % less than the cited reference, whereas the maximum drifts of the first and second floors were 5 % and 3.3 % less. Although the employed reference has no information regarding an additional damping ratio, a supplemental damping ratio of 25 % was obtained in this study. A good correlation was obtained by the proposed method.

5.2.2. Five-storey building model

A five-storey building has been investigated for different gap distances and ground motions. Linear (LVD) and nonlinear viscous dampers (NVD) were implemented on the structure. NVDs produce a lower damping force between damper ends than LVDs for the same structural velocity response. This situation is due to the velocity exponent (α). The velocity exponent takes values between 0 and 1. Different damper types and their forces based on the velocity exponent are given in Figure 8.

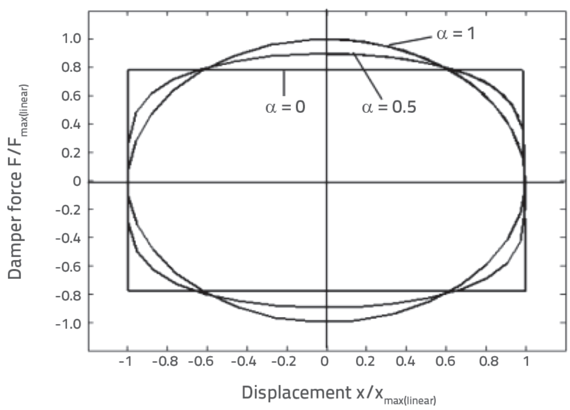

Figure 8. Damper force–displacement ratio for friction (α = 0), NV (α = 0.5) and LV (α = 1) dampers[29]

Equation 10 was used to calculate the damping coefficient of NVDs [53]:

Table 2. Comparative results of total damper sizes

	Lavan and Levy (2005)	Proposed method
Total damper coefficient [kNs/m]	1522.2	1397.5 (-8.1 %)
Maximum drifts (first and second floors)	9.0 and 9.0 mm	8.5 and 8.7 mm

Table 3. Supplemental damper sizes (×10⁶ Ns/m) and ratios

Earthquake name, year	Station (component)	10 cm			15 cm		
		ξ_d	cd(1)	cd(0.5)	ξ_d	cd(1)	cd(0.5)
Chi-Chi, 1999	TCU065 (E)	75	8.62	6.67	50	5.74	5.44
	TCU065 (N)	60	6.89	5.33	25	2.87	2.72
Imperial Valley, 1979	Array #5 (140)	-	-	-	-	-	-
	Array #7 (140)	45	5.17	4.90	5.	0.57	0.54
Kobe, 1995	Takatori (0)	85	9.77	7.56	75	8.62	8.17
	Takatori (90)	90	10.3	7.97	85	9.77	9.26
Kocaeli, 1999	Duzce (180)	15	1.72	1.33	-	-	-
	Duzce (270)	50	5.74	4.44	10	1.15	1.09
Landers, 1992	Lucerne (260)	25	2.87	2.22	-	-	-
	Lucerne (345)	-	-	-	-	-	-
Northridge, 1994	Rinaldi (228)	95	11.1	8.59	65	7.47	7.08
	Rinaldi (318)	85	9.77	7.56	45	5.17	4.90

$$cd(a) = \frac{cd(1)(\omega_1 \cdot x_0)^{1-\alpha}}{\beta} \tag{10}$$

Where $cd(1)$ is the linear damper coefficient, ω_1 is the first natural frequency of the building, x_0 is the maximum drift, and β is calculated as follows:

$$\beta = \frac{2^{2+\alpha}\Gamma^2(1+\alpha/2)}{\pi\Gamma(2+\alpha)} \tag{11}$$

Where Γ is the gamma function. In this study, the velocity exponent (α) was assumed to be 0.5. Table 3 demonstrates the supplemental damping ratios (ξ_d) and linear $cd(1)$ and nonlinear $cd(0.5)$ viscous damper sizes.

The structures with viscous dampers have additional damping without additional rigidity because of these devices. This feature results in the same frequencies for the structure for an adequate seismic gap after the installation of viscous dampers with a sufficient damping coefficient. Therefore, the wavelet coherence approach is adequate for determining the viscous damper size that prevents pounding using the acceleration responses of the structure with and without an appropriate separation.

Table 3 shows the optimum damper sizes and ratios under various earthquake motions. Damper sizes are not available for the Imperial Valley (Array #5) and Landers (Lucerne 345) earthquakes for both gap distances and Kocaeli (Duzce 180) earthquakes for the gap of 15 cm because there is no pounding. The maximum damper coefficient was obtained in the Northridge earthquake (Rinaldi 228). The total damper size decreased as the gap size increased. Nonlinear dampers reduce the damping coefficients by 22.6 and 5.23 % when the gap distances are 10 and 15 cm, respectively. This rate is the same for all earthquakes. An examination of Eq. 10 shows that the maximum drift (x_0) is the only variable when the NVD size is calculated from LVD. Therefore, in this study, as the building collides with a rigid wall, maximum drift (x_0) is equal to the separation distance for each ground motion.

6. Conclusions

Signal processing tools are becoming important and being applied in seismic engineering. Knowledge gained through the convolution of seismic signals, such as ground motions or structural responses, can provide insight into the dynamic behaviour of seismic activity. The proposed method is not only an alternative to existing methods but it also has a lower computational load and is easier to understand. This study has shown that wavelet coherence can be used to identify seismic pounding. In addition, optimum damper sizes for preventing pounding during seismic activity were obtained by simulating seismic responses with and without pounding and obtaining their frequency properties. The conclusions of this study can be summarized as follows:

- When a structure is exposed to collisions, wavelet coherence coefficients for shorter periods are low, indicating the low coherence between acceleration responses with and without pounding verifying that pounding is present.
- Wavelet coherence analysis can be used to identify the exact moment of pounding. In addition, the more blue the coherence spectrum, the more severe is the pounding force. Thus, WCoh plots can be used to obtain pounding force information without using one of the various models in the literature.
- The wavelet coherence method is a promising tool for obtaining viscous damper size using only seismic responses. It has a high computation speed and is easy to understand.
- Nonlinear viscous dampers have a damping ratio that is identical to that of linear viscous dampers while having a lower damping force, thereby protecting the structure and damper device at high structural velocities.

REFERENCES

[1] Hong, H.P., Wang, S.S., Hong, P.: Critical building separation distance in reducing pounding risk under earthquake excitation, Structural Safety, 25 (2003) 3, pp. 287-303, https://doi.org/10.1016/S0167-4730(02)00080-2.

[2] Lin, J.H.: Evaluation of critical separation distance to avoid seismic pounding between buildings: A spectral approach, Earthquake Engineering and Structural Dynamics, 50 (2021) 11, pp. 2863-3882, https://doi.org/10.1002/eqe.3476

[3] Penzien, J.: Evaluation of building separation distance required to prevent pounding during strong earthquakes, Earthquake Engineering and Structural Dynamics, 26 (1998) 8, pp. 849-858, https://doi.org/10.1002/(SICI)1096-9845(199708)26:8<849::AID-EQE680>3.0.CO;2-M

[4] Khatami, S.M., Naderpour, H., Mortezaei, A., Razavi, S.M.N., Lasowicz, N., Jankowski, R.: Effective gap size index for determination of optimum separation distance preventing pounding between buildings during earthquakes, Applied Sciences, 11 (2021) 5, 2322, https://doi.org/10.3390/app11052322

[5] Jankowski, R., Seleemah, A., El-Khoriby, S., Elwardany, H.: Experimental study on pounding between structures during damaging earthquakes, Key Engineering Materials, 627 (2015), pp. 249-252, https://doi.org/10.4028/www.scientific.net/KEM.627.249

[6] Xue, Q., Zhang, C., He, J., Zou, G., Zhang, J.: An Updated Analytical Structural Pounding Force Model Based on Viscoelasticity of Materials, Shock and Vibration, 2016 (2016), Article ID 2596923, 15 pages, https://doi.org/10.1155/2016/2596923

[7] Anagnostopoulos, S.A.: Pounding of buildings in series during earthquakes, Earthquake Engineering & Structural Dynamics, 16 (1988) 3, pp. 443-456, https://doi.org/10.1002/eqe.4290160311

[8] Davis, R.O.: Pounding of buildings modelled by an impact oscillator. Earthquake Engineering & Structural Dynamics, 21 (1992) 3, pp. 253-274, https://doi.org/10.1002/eqe.4290210305

[9] Pantelides, C.P., Ma, X.: Linear and nonlinear pounding of structural systems, Computers and Structures, 66 (1998) 1, pp. 79-92, https://doi.org/10.1016/S0045-7949(97)00045-X

[10] Karayannis, C.G., Favvata, M.J.: Earthquake-induced interaction between adjacent reinforced concrete structures with non-equal heights, Earthquake Engineering and Structural Dynamics, 34 (2005) 1, pp. 1-20, https://doi.org/10.1002/eqe.398

[11] Jankowski, R.: Non-linear viscoelastic modelling of earthquake-induced structural pounding, Earthquake Engineering and Structural Dynamics, 34 (2005) 6, pp. 595-611, https://doi.org/10.1002/eqe.434

[12] Mahmoud, S., Jankowski, R.: Elastic and inelastic multi-storey buildings under earthquake excitation with the effect of pounding, Journal of Applied Sciences, 9 (2009) 18, pp. 3250-3262, https://doi.org/10.3923/jas.2009.3250.3262

[13] Khatiwada, S., Chouw, N., Butterworth, J.W.: A generic structural pounding model using numerically exact displacement proportional damping, Engineering Structures, 62–63 (2014) pp. 33-41, https://doi.org/10.1016/j.engstruct.2014.01.016

[14] Aida, T., Aso, T., Takeshita, K., Takiuchi, T., Fujii, T.: Improvement of the structure damping performance by interconnection, Journal of Sound and Vibration, 242 (2001) 2, pp. 333-353, https://doi.org/10.1006/jsvi.2000.3349

[15] Ying, Z.G., Ni, Y.Q., Ko, J.M.: Non-linear stochastic optimal control for coupled-structures system of multi-degree-of-freedom, Journal of Sound and Vibration, 274 (2004) 3–5, pp. 843-861, https://doi.org/10.1016/S0022-460X(03)00610-2

[16] Basili, M., de Angelis, M.: Optimal passive control of adjacent structures interconnected with nonlinear hysteretic devices, Journal of Sound and Vibration, 301 (2007) 1–2, pp. 106-125, https://doi.org/10.1016/j.jsv.2006.09.027

[17] Park, K.S., Ok, S.Y.: Hybrid control approach for seismic coupling of two similar adjacent structures, Journal of Sound and Vibration, 349 (2015), pp. 1-17, https://doi.org/10.1016/j.jsv.2015.03.028

[18] Palermo, M., Silvestri, S.: Damping reduction factors for adjacent buildings connected by fluid-viscous dampers. Soil Dynamics and Earthquake Engineering, 138 (2020), 106323, https://doi.org/10.1016/j.soildyn.2020.106323

[19] Trombetti, T., Silvestri, S.: Novel schemes for inserting seismic dampers in shear-type systems based upon the mass proportional component of the Rayleigh damping matrix, Journal of Sound and Vibration, 302 (2007) 3, pp. 486-526, https://doi.org/10.1016/j.jsv.2006.11.030

[20] Miari, M., Choong, K.K., Jankowski, R.: Seismic pounding between adjacent buildings: Identification of parameters, soil interaction issues and mitigation measures, Soil Dynamics and Earthquake Engineering, 121 (2019), pp. 135-150, https://doi.org/10.1016/j.soildyn.2019.02.024

[21] López-Almansa, F., Kharazian, A.: Parametric study of seismic pounding between RC buildings with aligned slabs, Soil Dynamics and Earthquake Engineering, 125 (2019) 105718, https://doi.org/10.1016/j.soildyn.2019.105718

[22] Farahani, D., Behnamfar, F., Sayyadpour, H., Ghandil, M.: Seismic impact between adjacent torsionally coupled buildings, Soil Dynamics and Earthquake Engineering, 117 (2019), pp. 81-95, https://doi.org/10.1016/j.soildyn.2018.11.015

[23] Madani, B., Behnamfar, F., Tajmir Riahi, H.: Dynamic response of structures subjected to pounding and structure-soil-structure interaction, Soil Dynamics and Earthquake Engineering, 78 (2015), pp. 46-60, https://doi.org/10.1016/j.soildyn.2015.07.002

[24] Jia, H.Y., Lan, X.L., Zheng, S.X., Li, L.P., Liu, C.Q.: Assessment on required separation length between adjacent bridge segments to avoid pounding, Soil Dynamics and Earthquake Engineering, 120 (2019), pp. 398-407, https://doi.org/10.1016/j.soildyn.2019.01.031

[25] Torrence, C., Compo, G.P.: A Practical Guide to Wavelet Analysis, Bulletin of the American Meteorological Society, 79 (1998) 1, pp. 61-78, https://doi.org/10.1175/1520-0477(1998)079<0061:APGTWA>2.0.CO;2

[26] Mohebi, B., Yazdanpanah, O., Kazemi, F., Formisano, A.: Seismic damage diagnosis in adjacent steel and RC MRFs considering pounding effects through improved wavelet-based damage-sensitive feature, Journal of Building Engineering, 33 (2021), 101847, https://doi.org/10.1016/j.jobe.2020.101847

[27] Xing, S., Halling, M.W., Meng, Q.: Structural pounding detection by using wavelet scalogram, Advances in Acoustics and Vibration (2012) Article ID 805141, 10 pages, https://doi.org/10.1155/2012/805141

[28] Young Noh, H., Krishnan Nair, K., Lignos, D.G., Kiremidjian, A.S.: Use of Wavelet-Based Damage-Sensitive Features for Structural Damage Diagnosis Using Strong Motion Data, Journal of Structural Engineering, 137 (2011) 10, https://doi.org/10.1061/(ASCE)ST.1943-541X.0000385

[29] Yazdanpanah, O., Formisano, A., Chang, M., Mohebi, B.: Fragility curves for seismic damage assessment in regular and irregular MRFs using improved wavelet-based damage index, Measurement: Journal of the International Measurement Confederation, 182 (2021), 109558, https://doi.org/10.1016/j.measurement.2021.109558

[30] De Domenico, D., Ricciardi, G., Takewaki, I.: Design strategies of viscous dampers for seismic protection of building structures: a review, Soil dynamics and earthquake engineering, 118 (2019), pp. 144-165, https://doi.org/10.1016/j.soildyn.2018.12.024

[31] Silvestri, S., Gasparini, G., Trombetti, T.: A five-step procedure for the dimensioning of viscous dampers to be inserted in building structures, Journal of Earthquake Engineering, 14 (2010) 3, pp. 417-447, https://doi.org/10.1080/13632460903093891

[32] Lavan, O., Levy, R.: Optimal design of supplemental viscous dampers for linear framed structures, Earthquake Engineering and Structural Dynamics, 35 (2006) 3, pp. 337-356, https://doi.org/10.1002/eqe.524

[33] Kandemir-Mazanoglu, E.C., Mazanoglu, K.: An optimization study for viscous dampers between adjacent buildings, Mechanical Systems and Signal Processing, 89 (2017), pp. 88-96, https://doi.org/10.1016/j.ymssp.2016.06.001

[34] Anagnostopoulos, S.A.: Pounding of buildings in series during earthquakes, Earthquake Engineering and Structural Dynamics, 16 (1988) 3, pp. 443-456, https://doi.org/10.1002/eqe.4290160311

[35] Davis, R.: Pounding of buildings modelled by an impact oscillator, Earthquake Engineering and Structural Dynamics, 21 (1992), pp. 253-274, https://doi.org/10.1002/eqe.4290210305

[36] Pantelides, C.P., Ma, X.: Linear and nonlinear pounding of structural systems, Computers and Structures, 6 (1998) 1, pp. 79-92, https://doi.org/10.1016/S0045-7949(97)00045-X

[37] Karayannis, C.G., Favvata, M.J.: Earthquake-induced interaction between adjacent reinforced concrete structures with non-equal heights, Earthquake Engineering and Structural Dynamics, 34 (2005) 1, pp. 1-20, https://doi.org/10.1002/eqe.398

[38] Mahdavi, S.H., Rofooei, F.R., Sadollah, A., Xu, C.: A wavelet-based scheme for impact identification of framed structures using combined genetic and water cycle algorithms, Journal of Sound and Vibration, 443 (2019), pp. 25-46, https://doi.org/10.1016/j.jsv.2018.11.022

[39] Maniatakis, C.A., Spyrakos, C.C., Kiriakopoulos, P.D., Tsellos, K.P.: Seismic response of a historic church considering pounding phenomena, Bulletin of Earthquake Engineering, 16 (2018), pp. 2913–2941, https://doi.org/10.1007/s10518-017-0293-5

[40] Hwang, S.H., Lignos, D.G.: Nonmodel-based framework for rapid seismic risk and loss assessment of instrumented steel buildings, Engineering Structures, 156 (2018), pp. 417-432, https://doi.org/10.1016/j.engstruct.2017.11.045

[41] Misiti, M., Misiti, Y., Oppenheim, G., Poggi, J.M.: MathWorks Wavelet Toolbox User's Guide, MathWorks Inc.: Natick, MA, USA, 2015.

[42] Chun, L.C., Zhengding, Q.: A method based on Morlet wavelet for extracting vibration signal envelope, 5th International Conference on Signal Processing Proceedings, 16th World Computer Congress, pp. 337-340, 2000.

[43] Sheen, Y.T., Hung, C.K.: Constructing a wavelet-based envelope function for vibration signal analysis, Mechanical Systems and Signal Processing, 18 (2004) 1, pp. 119-126, https://doi.org/10.1016/S0888-3270(03)00046-3

[44] Heidari, A., Majidi, N.: Earthquake acceleration analysis using wavelet method, Earthquake Engineering and Engineering Vibration, 20 (2021) 1, pp. 113-126, https://doi.org/10.1007/s11803-021-2009-8

[45] Lin, J., Qu, L.: Feature extraction based on morlet wavelet and its application for mechanical fault diagnosis, Journal of Sound and Vibration, 234 (2000) 1, pp. 135-148, https://doi.org/10.1006/jsvi.2000.2864

[46] Grinsted, A., Moore, J.C., Jevrejeva, S.: Application of the cross wavelet transform and wavelet coherence to geophysical time series, Nonlinear Processes in Geophysics, 11 (2004) 5/6, pp. 561-566, https://doi.org/10.5194/npg-11-561-2004, 2004

[47] Aksoylu, C., Mobark, A., Arslan, M.H., Erkan, I.H.: A comparative study on ASCE 7-16, TBEC-2018 and TEC-2007 for reinforced concrete buildings, Revista de La Construccion, 19 (2020) 2, pp. 282–305, https://doi.org/10.7764/rdlc.19.2.282-305

[48] The Math Works, Inc. MATLAB. Version 2022a, The Math Works, Inc., 2022.

[49] Azevedo, J., Bento, R.: Design criteria for buildings subjected to pounding, Eleventh World Conference on Earthquake Engineering, Acapulco, Mexico, pp. 23-28, 1996.

[50] Gu, X., Jamshidi, S., Sun, H.G., Niyogi, D.: Identifying multivariate controls of soil moisture variations using multiple wavelet coherence in the U.S. Midwest, Journal of Hydrology, 602 (2021) 126755, https://doi.org/10.1016/j.jhydrol.2021.126755

[51] De Domenico, D., Ricciardi, G., Takewaki, I.: Design strategies of viscous dampers for seismic protection of building structures: A review, Soil Dynamics and Earthquake Engineering, 118 (2019), pp. 144-165, https://doi.org/10.1016/j.soildyn.2018.12.024

[52] Federal Emergency Management Agency (FEMA 1997). NEHRP guidelines for the seismic rehabilitation of buildings. Rep. No. 273/274, Building Seismic Safety Council, Washington, D.C.

[53] Martinez-Rodrigo, M., Romero, M.L.: An optimum retrofit strategy for moment resisting frames with nonlinear viscous dampers for seismic applications, Engineering Structures, 25 (2003) 7, pp. 913-925, https://doi.org/10.1016/S0141-0296(03)00025-7